Inductive Measurement of Plasma Jet Electrical Conductivity

(MSFC Center Director's Discretionary Fund Final Report; Part II, Project No. 99-24)

M.W. Turner and C.W. Hawk
University of Alabama in Huntsville, Huntsville, Alabama

R.J. Litchford
Marshall Space Flight Center, Marshall Space Flight Center, Alabama

Acknowledgments

This Technical Publication has been reviewed and is approved.

Garry M. Lyles
Manager
TD15/ASTP
Marshall Space Flight Center

TABLE OF CONTENTS

LIST OF FIGURES

LIST OF FIGURES (Continued)

LIST OF TABLES

LIST OF ACRONYMS AND SYMBOLS

Al	aluminum
C4	composition–4
emf	electromotive force
He	helium
HEDM	high-energy density matter
MHD	magnetohydrodynamic
TP	technical publication

NOMENCLATURE

0	appropriate characteristic value for the problem (subscript)
B_{app}	applied magnetic induction
B_{ind}	induced magnetic induction
D_m	magnetic diffusivity
$\mathbf{f}$	$m \times 1$ column matrix
$f(\xi)$	distribution function
$\mathbf{g}$	$n \times 1$ column matrix
$g(s)$	measured signal
$\mathbf{H}$	constraint matrix
$\mathbf{I}$	identify matrix
I	field coil current during a test
I_c	field coil current during calibration
I_{sp}	specific impulse
$\mathbf{K}$	$n \times m$ kernel matrix
$\mathbf{K}^T$	transpose of $\mathbf{K}$
$K(s,\xi)$	kernel
l	length of the conductive region behind the shock
L	inductance
L_0	characteristic length of the reactor
R	resistance
R_d	damping resistance
R_m	magnetic Reynolds number
s	distance from the search coil to the shock
t	time

NOMENCLATURE (Continued)

u	particle velocity behind the shock
u_0	characteristic plasma velocity
u_c	velocity of the calibration slug
U	velocity of the shock
V_c	calibration response function or kernel
V_{cp}	peak value of calibration slug response
V_p	peak value of the calculated voltage curve
$V(s)$	output signal of the search coil
x	distance from the search coil to an arbitrary point behind the shock
δ	differential change
γ	smoothing parameter
ε	finite measurement error
λ_i	ith eigenvalue of the covariance matrix
μ	magnetic permeability
$\xi=s-x$	distance from an arbitrary location x to the shock
ρ	resistivity
σ	electrical conductivity
σ^*	maximum conductivity
σ_0	characteristic plasma electrical conductivity
σ_c	calibration slug conductivity
Φ	pulse area of measured voltage curve
$\Phi(s)$	integrated-induced voltage signal
Φ_c	pulse area of calibration slug response function
ψ_1	function dependent on the conductivity distribution
ψ_2	function dependent on the conductivity distribution

TECHNICAL PUBLICATION

INDUCTIVE MEASUREMENT OF PLASMA JET ELECTRICAL CONDUCTIVITY
(MSFC Center Director's Discretionary Fund Final Report; Part II, Project No. 99–24)

1. INTRODUCTION

The need for fast, efficient interplanetary transport has led to the serious consideration of various concepts for nuclear/chemical pulsed propulsion and power. It is believed, for instance, that propulsion systems of this type are within the grasp of modern technical capability and can eventually yield the rapid acceleration and high specific impulse (I_{sp}) attributes that are deemed necessary. Actual success, of course, will depend upon the ability to overcome practical technical issues. For example, these concepts rest on the assumption that low-yield microfusion/fission detonations or chemical detonations using high-energy density matter (HEDM) can eventually be realized in practice and that enabling technologies such as high-power standoff drivers and simple, effective reactor designs can be developed.

The simplest reactor design for propulsion is a pusher plate that physically interacts with the blast wave from the detonation. However, more intricate reactor schemes can be conceived in which the expanding diamagnetic plasma is forced to interact with an applied magnetic field. Reactors of this type can accomplish two important functions: (1) Collimation and reflection of the hot diamagnetic plasma for direct thrust production with minimal ablative effects and (2) electric power generation by direct energy conversion.

Specific pulsed magnetic flux compression reactor concepts are, in fact, currently being considered for spacecraft propulsion and power.[1] In these devices, the expanding diamagnetic plasma cloud compresses the initial magnetic flux within a semi-enclosed reactor structure until the expansion is ultimately reversed by increasing magnetic pressure. The detonation products are then collimated and expelled, and electrical power can be inductively extracted.

Of crucial importance to the complex underlying magnetohydrodynamic (MHD) processes in field compression reactors is the magnetic Reynolds number (R_m), the value of which depends upon the product of plasma electrical conductivity and velocity. Indeed, flux diffusion losses into the plasma will be severe unless $R_m \gg 1$. As such, a thorough understanding of MHD phenomena at high R_m is essential to the design of flux compression reactors as well as explosively driven MHD converters.

Explosive sources offer a simple and convenient method for producing high-speed, highly conductive plasma jets, and it is contended that these sources represent a path for conducting meaningful nonnuclear demonstration tests. The Mark I device envisioned by Litchford et al., for instance, is shown schematically in figure 1.[1] This is a radial-mode flux compression reactor which uses colliding plasma jets from opposing high-explosive charges to produce a radially expanding plasma armature. The plasma armature is then used to compress a trapped magnetic field against a conductive stator surface. The Mark I configuration is intended to serve as a moderate scale ($1/2$-m-diameter) technology demonstrator as well as a low-cost expendable unit for supporting basic scientific investigations.
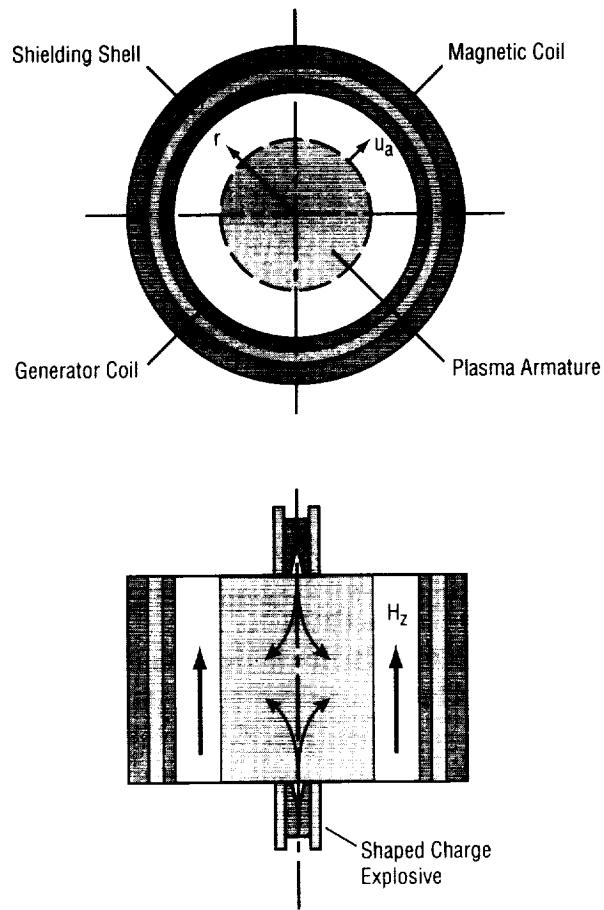
Figure 1. Mark I configuration for an explosively driven radial-mode magnetic flux compression reactor.[1] This device is intended to serve as a moderate-scale technology demonstrator as well as a low-cost expendable unit for supporting basic research.

As a step toward realizing this device, an effort has been initiated to explore the utilization of explosively driven plasma sources for compression of magnetic fields and to quantify achievable magnetic Reynolds number. Available empirical data for the electrical conductivity of explosive plasma jets are limited, but there is evidence to indicate that sufficiently high R_m can be produced.

For instance, experiments on 44° cavity charges of composition–4 (C4) by Burnham and Marshall have revealed that a cohesive plasma slug is ejected at speeds on the order of 3×10^4 m/sec with a core electrical conductivity of 10^4 S/m.[2–4] Collisional processes between colliding jets, as illustrated in figure 2, were also observed through high-speed photography. Independent explosive-driven MHD experiments by Jones and McKinnon indicated the production of R_m approaching unity in moderate-scale devices.[5] Explosive plasma sources developed by Baum and Shimmin have produced plasma flow velocities of 30 km/sec and conductivities of 30 kS/m, which in a laboratory-scale, 25-mm-diameter tube yields an R_m of 28.[6] The explosive compressor developed by Voitenko produces comparable shock velocities and is likely to have a comparable range of R_m.[7] Furthermore, a concept for explosive-driven collapse of a lined cylindrical cavity, as proposed by Koski et al., has shown considerable promise as well.[8–10]

2
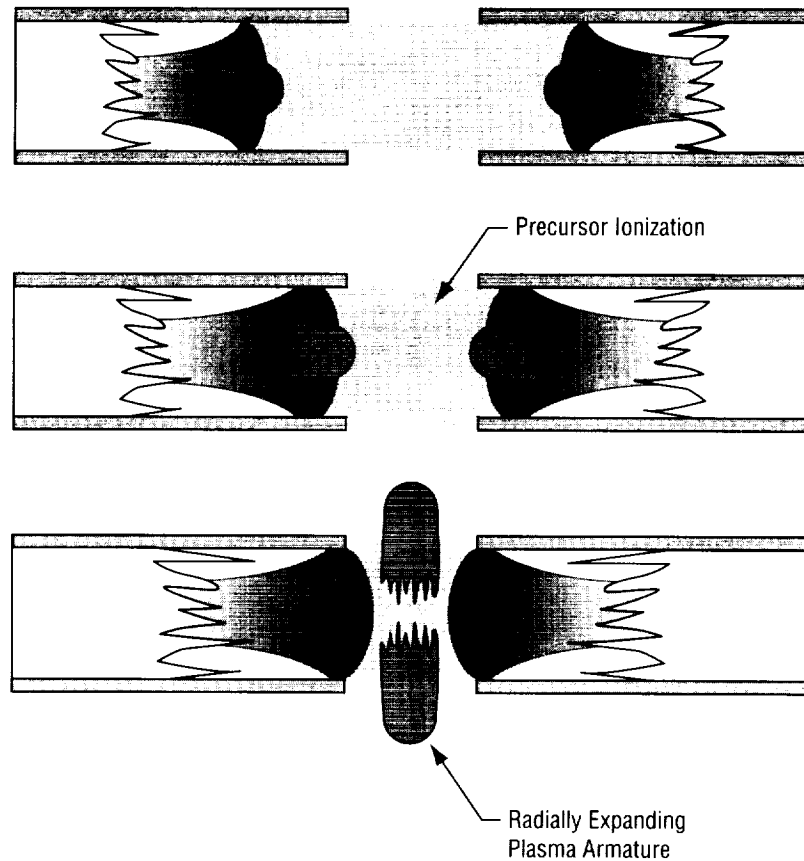
Figure 2. Illustration of plasma jet collisional process and radial armature formation.

Based on this evidence, research had proceeded with the development of a simple and reliable inductive probe for measuring the electrical conductivity of explosive plasma jets. A more direct approach using biased contact electrodes is possible, but it is well known that this methodology suffers from large surface resistances, and an electrodeless technique is preferred. Therefore, it was decided to adapt the inductive probing technique developed by Lin, Resler, and Kantrowitz for shock tube studies.[11] In this method, the perturbation of an applied magnetic field by a plasma jet induces a voltage in a search coil, which, in turn, can be used to infer electrical conductivity through the inversion of a Fredholm integral equation of the first kind. This technical publication (TP) describes the design, development, and calibration of a 1-in.-diameter probe and the results of exploratory experiments using plasma jets expelled from 15-g shaped charges formed from seeded and unseeded octol.

2. MAGNETIC DIFFUSION PHENOMENA

Some of the major plasmadynamic issues associated with detonation plasma-driven field compression are as follows: (1) Achieving sufficiently high expansion velocity and electrical conductivity to ensure diamagnetic behavior, (2) electron Joule heating effects, (3) field-aligned ion flow due to the ambipolar potential, (4) Rayleigh-Taylor surface instabilities, and (5) ensuring rebound of the plasma expansion. In this TP, the effects of magnetic diffusion, particularly with respect to explosively generated plasma sources, are of primary concern.

There are a number of alternative ways to visualize the interaction between a moving conductor and a magnetic field. Perhaps the most common means of describing the phenomena is in terms of distortion of magnetic field lines by the conductor entering the field region and subsequent diffusion of field lines into the conductor. For a finite electrical conductivity (σ), the field lines diffuse into the conductor at a rate governed by the magnetic diffusivity ($D_m = 1/\mu\sigma$) where μ is the magnetic permeability.

The diamagnetic properties of plasma jets can be quantitatively measured by the relative value of the magnetic Reynolds number, a parameter that naturally evolves from dimensional analysis of the MHD equations in the form

$$R_m = \frac{B_{ind}}{B_{app}} = \mu_0 \sigma_0 u_0 L_0 \ , \tag{1}$$

where 0 subscript denotes an appropriate characteristic value for the problem. Here, σ_0 is the characteristic plasma electrical conductivity, u_0 is the characteristic plasma velocity, and L_0 is a characteristic length of the reactor (e.g., diameter). In a general sense, R_m may be thought of as a relative measure of the induced magnetic induction in the plasma (B_{ind}) with respect to the external applied magnetic induction (B_{app}). According to the definition of magnetic diffusivity, it is inferred that the magnetic Reynolds number is inversely related to the magnetic diffusivity (D_m):

$$R_m = \frac{u_0 L_0}{D_m} \ . \tag{2}$$

The interaction between a moving conductor and a magnetic field may also be described in terms of eddy currents produced by gradients in the Faraday voltage. From this perspective, the eddy currents induce a perturbation field which, when added to the original field, distorts the field lines. The strength of the eddy current loops depends on the ratio of Faraday voltage to loop resistance, which may be shown to be proportional to R_m. Growth and decay of the eddy current loops are determined by the inductive L/R decay time of the current loop, which is directly related to the diffusion time.

Thus, it is clear that for magnetic Reynolds numbers greater than unity, where the induced field is at least as strong as the applied field, the plasma will be resistive to magnetic diffusion. That is, the induced

field associated with eddy currents in the plasma act in an opposing direction to the applied field, and if the induced field is high enough, the plasma interface effectively behaves as a magnetic compression surface.

The important point to note is that R_m depends primarily on the product σu such that one would desire high electrical conductivity and high expansion velocities in order to achieve low-flux diffusion losses. For nuclear detonations, both of these parameters are extremely high and $R_m \gg 1$, as desired. For conventional chemical detonations, the characteristic values are marginal and the plasma jet sources must be carefully designed to achieve $R_m > 1$.

3. THEORY OF INDUCTIVE PROBE

3.1 Fundamental Principles of Operation

The inductive probe, illustrated in figure 3, is a simple electromagnetic system consisting of two adjacent coils wound on a nonmagnetic tube. The field coil (i.e., solenoid) is first excited by the dc power supply in order to introduce an axisymmetric magnetic field inside the tube. The resulting field lines are illustrated in figure 3. A small search coil is situated slightly forward of the excitation coil to pick up the electromagnetic disturbance produced by passage of the plasma jet.
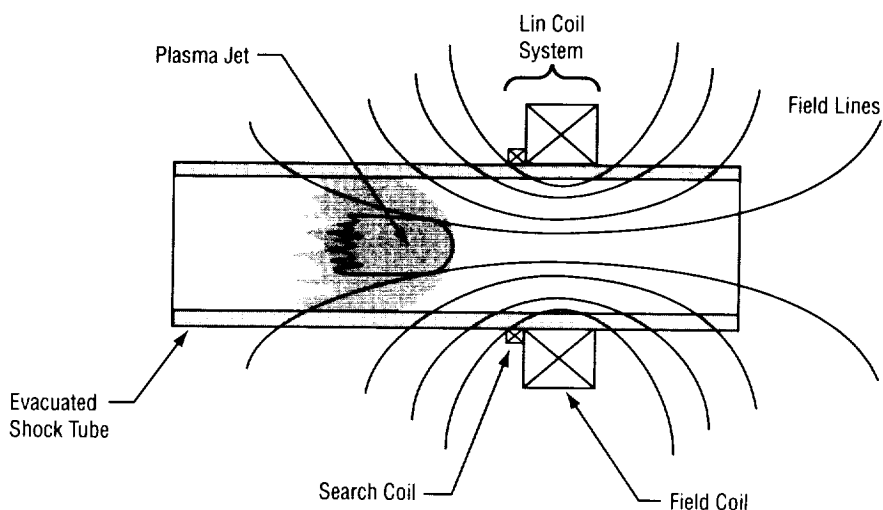

Figure 3. Illustration of inductive probe principle of operation. The plasma jet displaces the field lines of the excitation coil and induces an emf in the search coil. The degree of field displacement can be correlated with plasma jet electrical conductivity.

As the plasma jet enters the field region, it displaces the magnetic field lines due to its diamagnetic properties; that is, eddy currents are established in the plasma which resist magnetic field penetration. This perturbation or compression of the magnetic field lines induces an electromotive force (emf) in the search coil. The magnitude of the emf is representative of the degree of field displacement and, given the jet velocity, can be correlated with the plasma electrical conductivity. Actual recovery of the electrical conductivity distribution from the induced emf signal requires the difficult inversion of a Fredholm integral equation of the first kind, as shown in the following subsection devoted to the mathematical theory of probe operation.

In principle, the plasma conductivity can be directly calculated from the coil geometry and the known jet velocity; however, Lin et al. have demonstrated that it is much easier to obtain the probe response function empirically by firing a metallic slug of known conductivity through the device.[11]

3.2 Mathematical Theory of Operation

Following the mathematical analysis of Lin et al. for the inductive probe, a Fredholm integral equation of the first kind for the conductivity σ is arrived at:[11]

$$\Phi(s) = \frac{UuI}{u_c^2 I_c \sigma_c} \int_0^l V_c(s - \xi)\sigma(\xi)\, d\xi \ , \tag{3}$$

where $\Phi(s)$ is the integrated-induced voltage signal on the search coil

$$\Phi(s) = \int_0^s V(s)\, ds \ , \tag{4}$$

and $V(s)$ is the output signal of the search coil. A diagram of the parameters relevant to the mathematical analysis is given in figure 4. The major parameters are as follows: Length of the conductive region behind the shock (l), distance from the search coil to the shock (s), distance from the search coil to an arbitrary point behind the shock (x), distance from an arbitrary location x to the shock ($\xi = s - x$), velocity of the shock (U), particle velocity behind the shock (u), field current during a test (I), velocity of the calibration slug (u_c), field current during calibration (I_c), electrical conductivity of the calibration slug (σ_c), calibration response function or kernel (V_c), and the unknown plasma electrical conductivity distribution (σ).
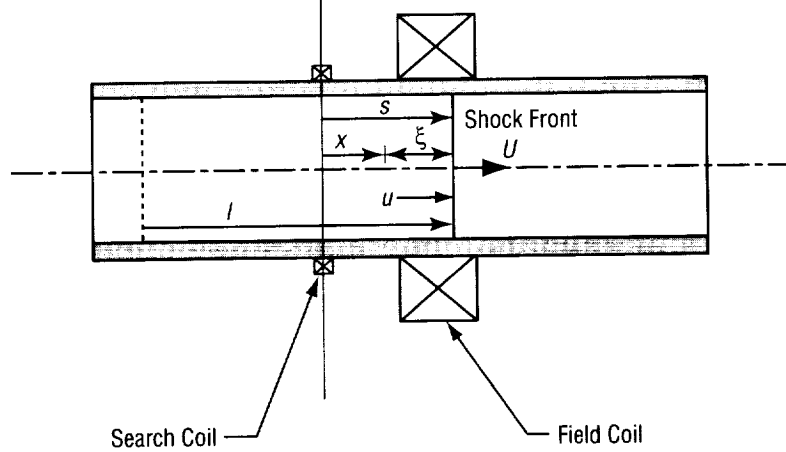

Figure 4. Diagram of parameters relevant to the mathematical analysis of probe operation.

8

The Fredholm integral equation of the first kind has the general form

$$g(s) = \int_a^b K(s,\xi) f(\xi) \, d\xi \ , \tag{5}$$

where $g(s)$ is a known function (i.e., the measured signal), $K(s,\xi)$ is the kernel, and $f(\xi)$ is the unknown distribution function. In general, closed-form analytical inversions can be obtained only for special functions, and one must resort to numerical methods.

Deconvolution algorithms for recovering $f(\xi)$ are generally based on a linear vector space representation in the form

$$g(s_i) = \sum_j K(s_i,\xi_j) f(\xi_j) \ , \tag{6}$$

which may be written in matrix form as

$$\mathbf{g} = \mathbf{Kf} \ , \tag{7}$$

where $\mathbf{g}$ is an $n \times 1$ column matrix, $\mathbf{f}$ is an $m \times 1$ column matrix, and $\mathbf{K}$ is an $n \times m$ matrix, which may include numerical quadrature coefficients. Multiplying through by $\mathbf{K}^T$ and inverting yields the desired distribution function

$$\mathbf{f} = \left(\mathbf{K}^T \mathbf{K}\right)^{-1} \cdot \mathbf{K}^T \cdot \mathbf{g} \ . \tag{8}$$

Unfortunately, this least-squares linear inversion is subject to instability because of the ill-conditioned kernel and because the kernel may exhibit linear dependence. Given a finite measurement error (ε), Twomey showed that the resulting error in $\mathbf{f}$ would be[12]

$$\left|\delta f(\xi)\right| = \sum_{i=1}^n \frac{\varepsilon_i^2}{\lambda_i} \ , \tag{9}$$

where λ_i is the ith eigenvalue of the covariance matrix defined by the product $\mathbf{KK}^T$. For relatively large off-diagonal terms, the eigenvalues can be extremely small and a finite measurement error ε can lead to a large error in $\mathbf{f}$.

A simple modification to least-squares linear inversion, known as constrained linear inversion, can sometimes avoid the severe instabilities and permit a reasonably accurate numerical inversion. A description of constrained linear inversion is given by Twomey.[12] Following Twomey's development, the following is obtained:

$$\mathbf{f} = \left(\mathbf{K}^T \mathbf{K} + \gamma \mathbf{H}\right)^{-1} \cdot \mathbf{K}^T \cdot \mathbf{g} \ , \tag{10}$$

9

where a constraint matrix **H** along with a Lagrange multiplier γ has been introduced, such that

$$0 \le \gamma < \infty \ . \tag{11}$$

It is easy to see that when $\gamma=0$, there is no smoothing and the least-squares linear inversion is recovered. When $\gamma \to \infty$, infinite smoothness is approached, such that all information is smeared away. As such, the desire is to have γ be as small as possible while also maintaining numerical stability. **H** can have different forms, depending on how one defines the smoothness. Using sum of squares as a smoothness indicator, **H** becomes the identity matrix

$$\mathbf{H} = \mathbf{I} \ . \tag{12}$$

In some cases, interpretation of the experimental data can be facilitated by an approximate treatment of the integral equation. For example, Lin et al. showed that it is possible to express the ratio between the maximum conductivity (σ^*) behind the shock wave and the calibration slug conductivity (σ_c) as

$$\frac{\sigma^*}{\sigma_c} = \frac{u_c I_c V_p}{U u I V_{cp}} \psi_1 \tag{13}$$

or

$$\frac{\sigma^*}{\sigma_c} = \frac{u_c^2 I_c \Phi}{U u I \Phi_c} \psi_2 \ , \tag{14}$$

where, respectively, V_{cp} and Φ_c are the peak and the pulse area of the calibration slug response function, V_p and Φ are the peak and the pulse area of the measured voltage curve, and ψ_1 and ψ_2 are functions dependent on the conductivity distribution. Various results for different conductivity distributions are tabulated in the literature.[11]

For the special case where the conductivity distribution is a step function and the probe response function is Gaussian, both ψ_1 and ψ_2 are unity. When the conductivity distribution deviates from a step function, both ψ_1 and ψ_2 can become complicated functions that may only be evaluated numerically. At any rate, it should be pointed out that when the variation of conducting is not too great, ψ_2 will be unity plus a small correction term. This behavior turns out to be quite fortuitous for the purpose of analyzing the plasma jets encountered in our experiments.

10

4. PROBE DEVELOPMENT

4.1 Design

The detailed design of the inductive probe is shown in figure 5. The basic structure is a nylon coil form that has been machined to accept two coil windings. The coil form has a bore diameter of 1.3 in. and a wall thickness of 0.125 in. A 900-turn magnet field coil was wound from No. 18 enameled magnet wire. The resulting solenoid has a length of 1.5 in. and an outer diameter of 3.8 in. The search coil consists of dual 25-turn windings of No. 28 enameled magnet wire. These windings can be connected in series or in a push-pull configuration as discussed below.
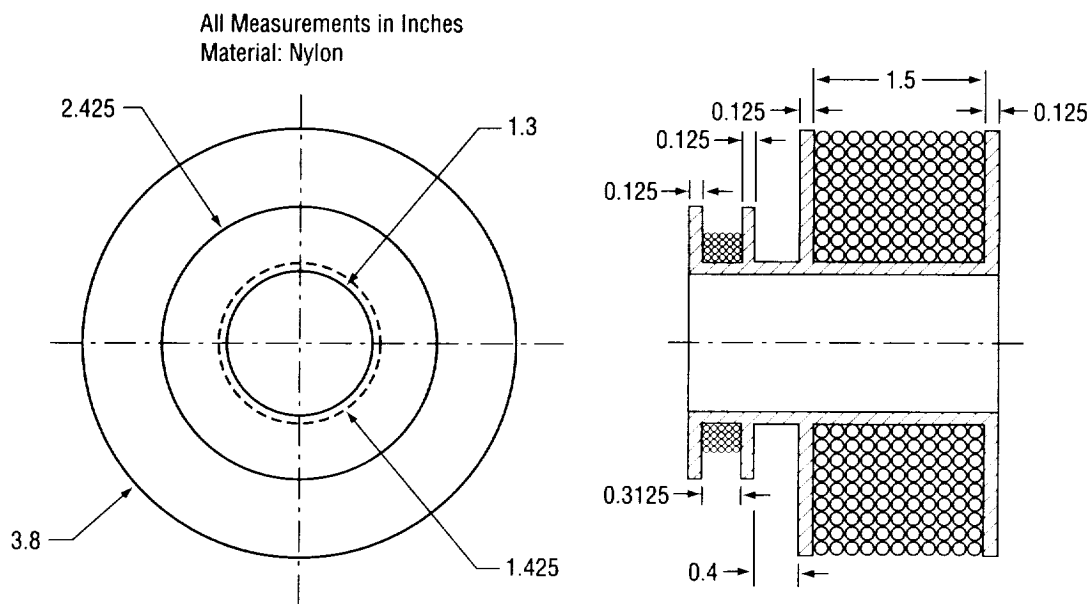

Figure 5. Detailed design drawing of probe.

The excitation field coil was designed to produce a solenoidal magnetic field between 0.5 and 1 T inside the bore. A 20-kW dc power supply was used to drive the excitation coil at 300 V (maximum), and the operating time was limited to 1 sec in order to minimize resistive heating.

The field coil was calibrated by measuring the time-varying current when activated by a solenoid switch. The time-varying magnetic field in the bore was also measured using a Hall probe connected to a Gauss meter. The resulting waveforms are shown in figure 6. A rise time of 20 msec, a peak current of 56 A, and a peak field intensity of 0.8 T was observed. Reproducibility of these waveforms was excellent. The waveforms remain relatively flat around the peak values for ≈15 msec after which they gradually decay and stabilize to ≈63 percent of their maximum values. Therefore, a 15-msec target window in which to probe the plasma jet at maximum field strength was available.
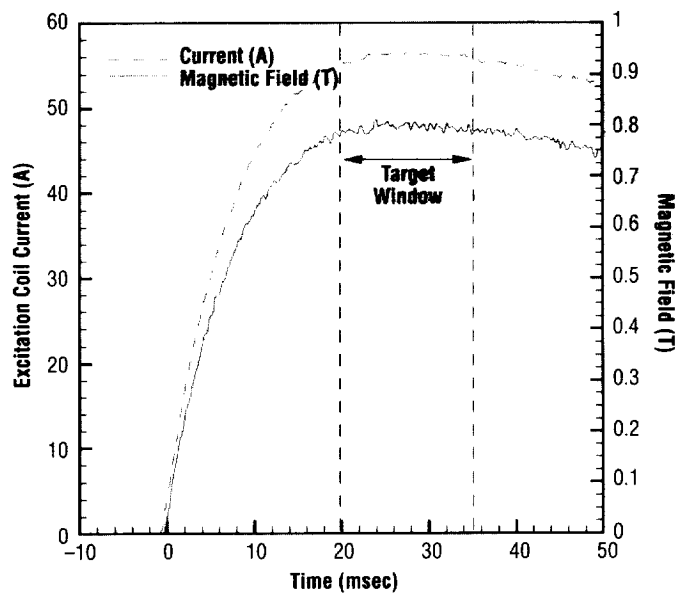
Figure 6. Measured coil current and field intensity waveforms.

In the shock tube experiments of Lin et al., electrostatic effects were encountered which were associated with nonuniform charge distributions in the ionized gas.[11] This effect, while of great physical interest, introduces a finite capacitance between the search coil and the plasma and could lead to spurious signals. This difficulty was overcome by connecting dual-turn windings in a push-pull configuration, as shown in figure 7. The center tap is connected to ground and 1 kΩ shunt resistors are used to achieve critical damping. In this configuration, the capacitive pickup from the two ends of the coil is canceled while the inductive pickup is unaffected. A similar strategy was implemented in the probe design so that either a 50-turn standard connection or a dual 25-turn push-pull connection could be utilized, as needed.
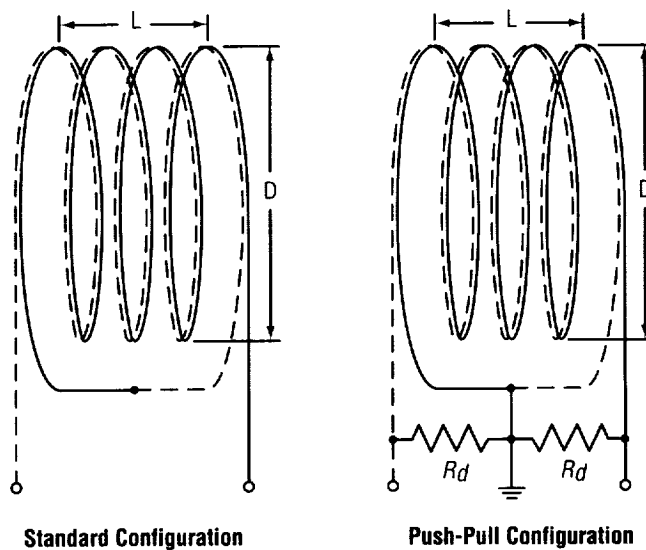

Figure 7. Illustration of standard and push-pull search coil configurations.
The critical damping resistance (R_d) is 1 kΩ.

4.2 Calibration

In order to calibrate the inductive probe, it is necessary to fire a metal slug of known electrical conductivity through the probe. The velocity of the slug must also be measured. To accomplish this requirement, a simple compressed gas gun using 150 lb/in² helium (He) stored in a small cylinder was developed. The helium was released into the gun breech by a solenoid actuated valve, which could be triggered electronically, and a 4-in.-long, 1-in.-diameter aluminum (Al) cylinder was propelled down a plastic barrel and through a glass tube holding the probe assembly. The resistivity of the aluminum was $\rho = 3 \times 10^{-8}$ $\Omega \cdot$m. The velocity of the slug was inferred from the deflection of a laser beam. A digital computer-controlled firing sequence was implemented incorporating appropriate timing delays, and the various signal waveforms were captured on a digital oscilloscope. A schematic of the experimental apparatus is shown in figure 8.
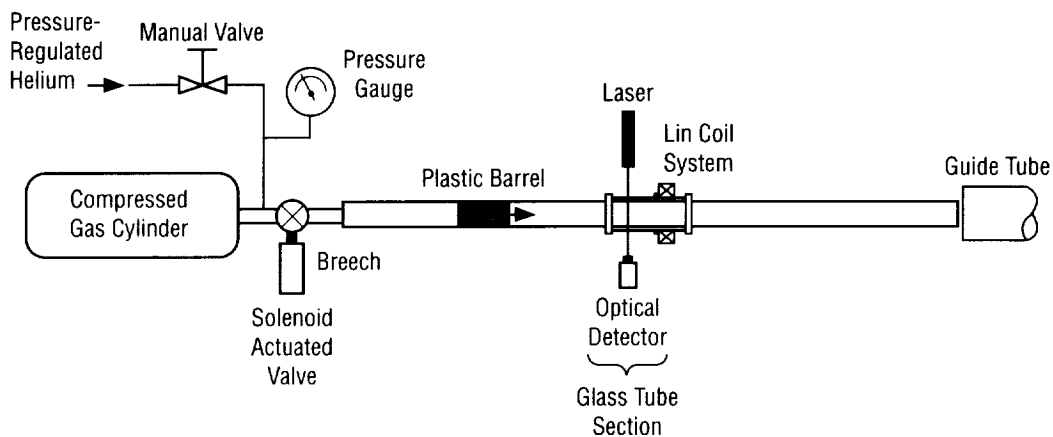

Figure 8. Schematic of experimental apparatus used for probe calibration. A light-gas gun was used to fire a 10-cm-diameter aluminum slug through the probe where velocity was inferred from the deflection of a laser beam.

The timing for the calibration experiment was crucial. For example, to hit the target window, it was necessary to accurately trigger the excitation field coil 20 msec before the slug entered the active probe region; otherwise, the probe would not be at maximum field strength at the appropriate moment. This timing problem was summarily resolved after several test shots.

To measure the slug velocity, a laser beam was directed through the glass tube and onto a fast response optical detector. When the slug entered the glass tube, the laser beam was deflected and the detector signal fell. After slug passage, the beam path was cleared and the detector signal returned to its normal value. Therefore, the time of flight of the slug past the beam could be determined and the velocity inferred from the known slug length. The captured detector waveforms are shown in figure 9 from which a time of flight of $\Delta t \approx 5$ msec was observed. A slug velocity of 2150 ± 164 cm/sec was deduced.
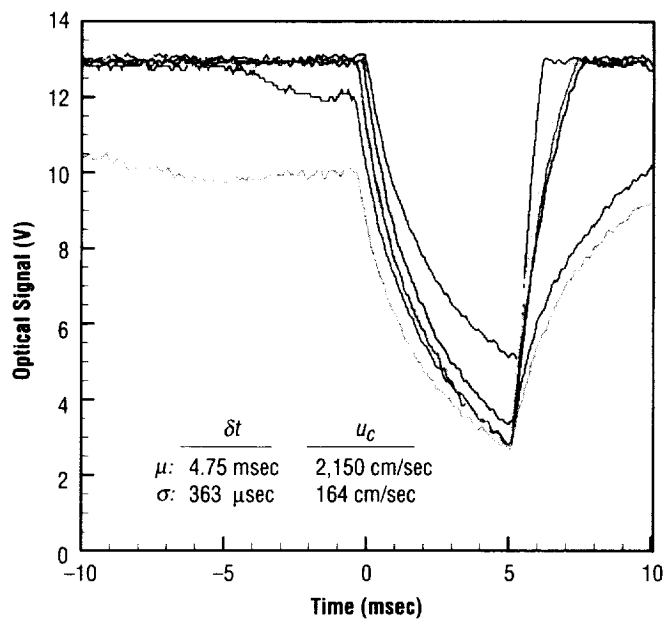
Figure 9. Time-of-flight waveforms from calibration experiments. Statistical parameters are indicated. Mean value–μ; standard deviation–σ.

The measured response function of the standard configuration search coil (50 turns) is shown in figure 10. This waveform, which represents an ensemble average of seven shots, consists of two perturbations. The first is the entrance perturbation associated with initial field displacement as the probe enters the active probe region. The second is the exit perturbation associated with restoration of the original field as the slug leaves the active probe region. When the slug fills the active region completely, there is no signal since the displaced field is quasi-steady. Only the entrance portion of the response function is needed for inversion purposes.
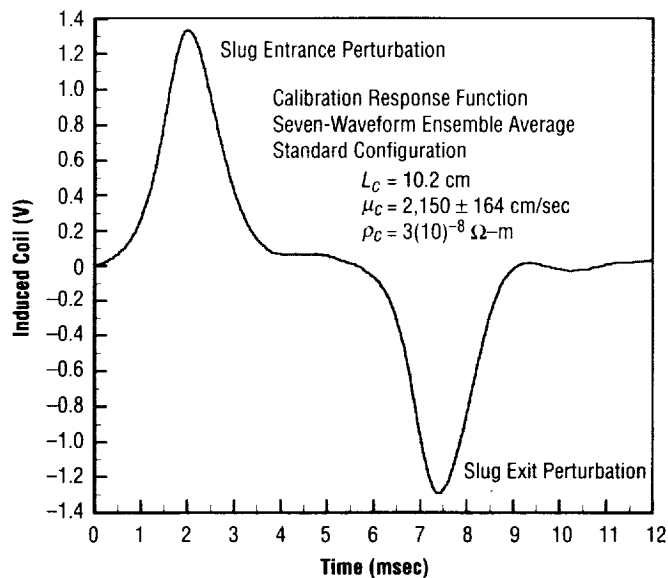

Figure 10. Measured response function for standard search coil configuration.

14
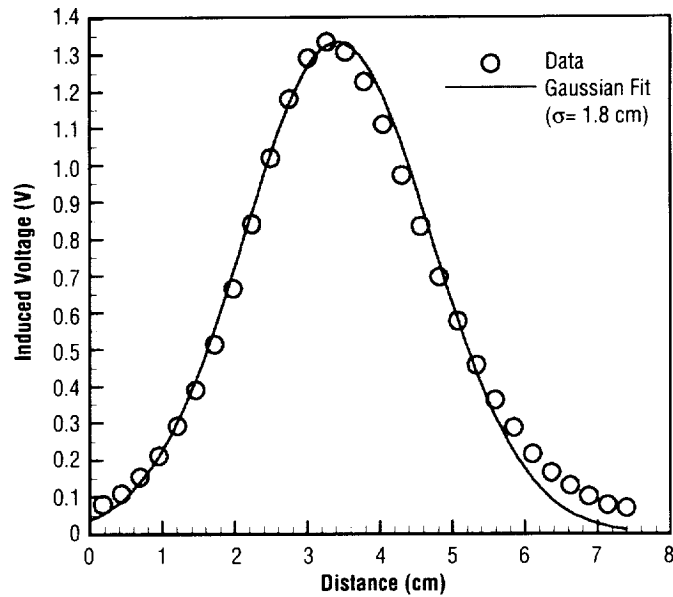
Figure 11. Gaussian fit of response function for standard search coil configuration.

The response function is nearly Gaussian as can be seen from the fit shown in figure 11. Here, transformation is made to spatial coordinates using the known slug velocity. The response function is observed to reach a peak value of ≈ 1.3 V when the leading edge of the slug is ≈ 3.5 cm past the search coil. The standard deviation of the Gaussian fit is 1.8 cm, indicating that the probe has an effective resolving power of ≈ 4 cm. This is more than sufficient to resolve the leading portion of a plasma jet.

The measured response functions for the push-pull search coil configuration (25-turn segments) is shown in figure 12. Again, these waveforms represent an ensemble average of seven independent shots. In this case, a response signal was obtained from each segment of the push-pull coil circuit where the output from each segment is referenced to the grounded center tap. Therefore, the entrance perturbation is positive for the push segment and negative for the pull segment. The exit perturbations are also of opposite sign.

The response functions are again found to be nearly Gaussian, and the peak signal values are exactly half of that obtained for the standard configuration, as expected. The effective resolving power is also identical to the standard configuration.

For the purpose of performing numerical inversions of the integral equation, Gaussian fits for the response function are always utilized. Use of experimental data points introduces unnecessary complexity and can even lead to numerical inaccuracies. This method is followed for both standard and push-pull configurations.

At this stage, a code for the constrained linear inversion technique was implemented and a validation calculation. The general approach was to use the aluminum slug response function in conjunction with a simulated Gaussian signal to test the algorithm. The simulated Gaussian signal was integrated to obtain $\Phi(s)$ and inversions were attempted in which $\mathbf{H} = \mathbf{I}$ and the smoothing parameter (γ) was varied over a wide range of values. In theory, a Gaussian response signal should deconvolve to a step function. The result of our inversion code is shown in figure 13 using $\gamma = 10^{-3}$.

15
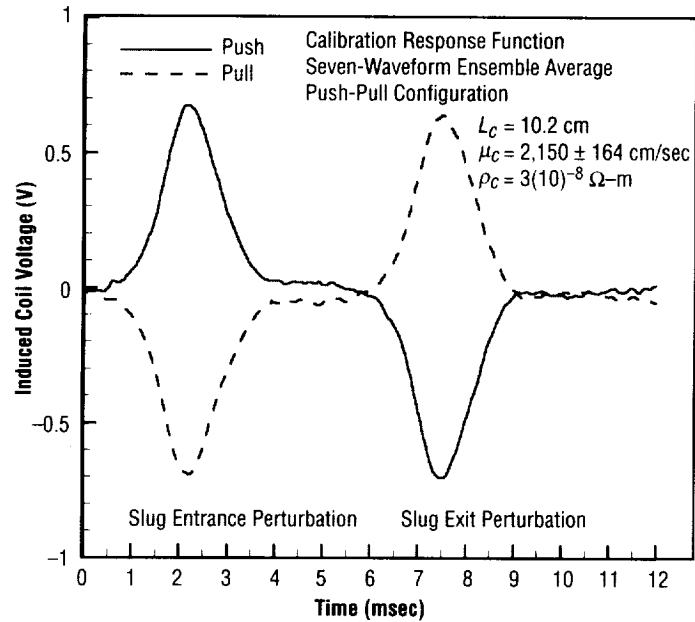
Figure 12. Measured response function for push-pull search coil configuration.
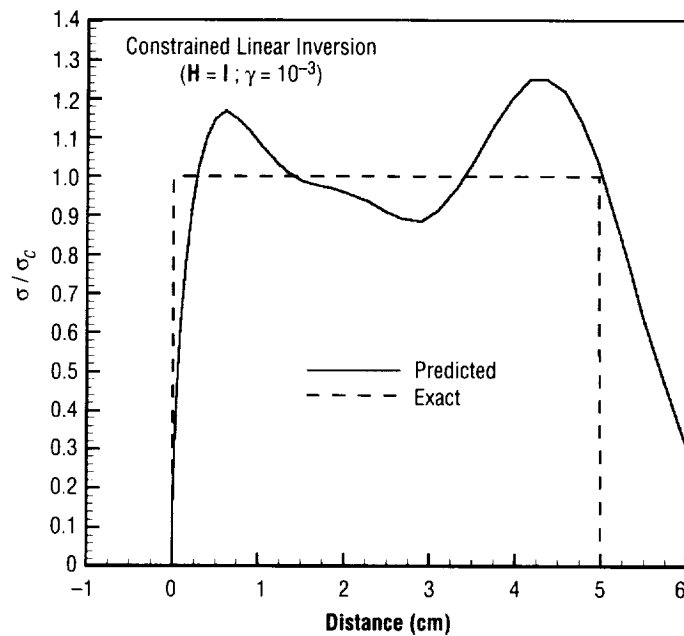
Figure 13. Validation calculations for constrained linear inversion technique.

The result is clearly not pleasing due to the overshoots and ringing errors, but the algorithm does produce a rough approximation. The Lagrange multiplier is close to zero but more smoothing is needed. Unfortunately, increasing the value of γ results in poorer performance. Additional modifications will be required to make this deconvolution algorithm sufficiently robust for reliable use.

16

5. PLASMA JET EXPERIMENTS

With probe development completed, exploratory laboratory experiments on explosive plasma jets were initiated. In these experiments, 15-g shaped charges (included cone angle of 44°) composed of octol (75 percent HMX/25 percent TNT) with various amounts of seed material (0-, 1-, and 2-percent potassium carbonate by mass) were investigated. Sample cast charges are shown photographically in figure 14. Note the change in colorization with seed fraction. All charges were prepared by Accurate Arms Company, McEwen, TN. Based on previous experiments with similar explosives, plasma jet velocities around 10 km/sec and electrical conductivities in the 10 kS/m range were anticipated.
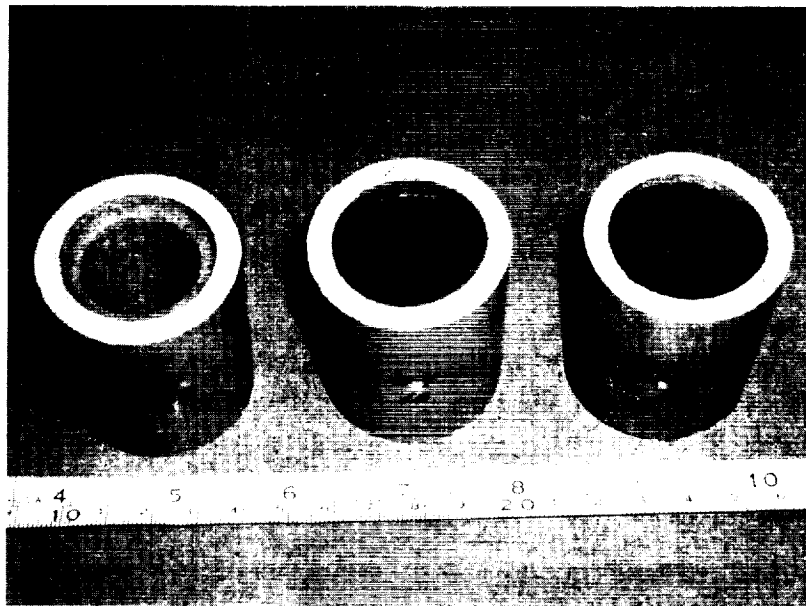

Figure 14. Photograph of cast octol shaped charges with 0-, 1-,
and 2-percent potassium carbonate seed by mass.

The simple experimental setup is illustrated in figure 15. Here, a shaped charge explosive is attached to a schedule 40 PVC pipe that includes a time-of-flight circuit and an inductive probe. The overall length of these expendable units was 40 in., and end caps were attached so that a rough vacuum in the pipe prior to a test could be established. The time-of-flight circuit consisted of two wires traversing the pipe with a separation distance of 10 cm. The first wire was located 8.5 in. from the shaped charge exit plane. A dc voltage (24 V) was applied to these wires, and the current was measured across appropriately sized ballast resistors. When the plasma jet broke each wire, the respective current signals would fall such that the time of flight between the two locations could be measured. A time of flight of 10 μsec for an estimated jet velocity of 10 km/sec was anticipated.

Expendable coil forms were fabricated and mounted to the PVC pipe and field coils and search coils were wound on these forms. The dimensions of these expendable probes were identical to those used in our calibration work. The probes were located 15 in. from the shaped charge exit plane.

17
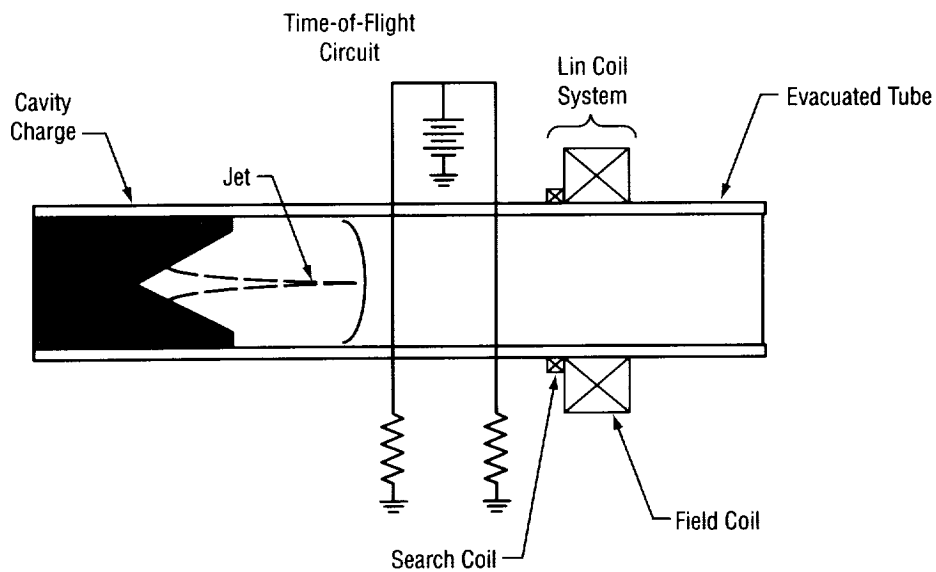
Figure 15. Schematic of expendable explosive units for measuring
plasma jet electrical conductivity.

The tests were conducted in a blast chamber located at Accurate Arms Company test facilities in Bucksnort, TN. To conduct a test, the assembled explosive units were placed in the chamber and a 200-msec delay initiator was attached to the end of the shaped charges as shown in figure 16. The delay initiator was necessary to ensure that the plasma jet passed through the probe during the desired target window at maximum field coil strength. It took slightly less than 200 msec for the solenoid-controlled relay to close. A rough vacuum would be established in the pipe, and a dual-circuit switch would be activated to excite the field coil and initiate the explosion. Data from the experiment were captured on a four-channel digital oscilloscope.
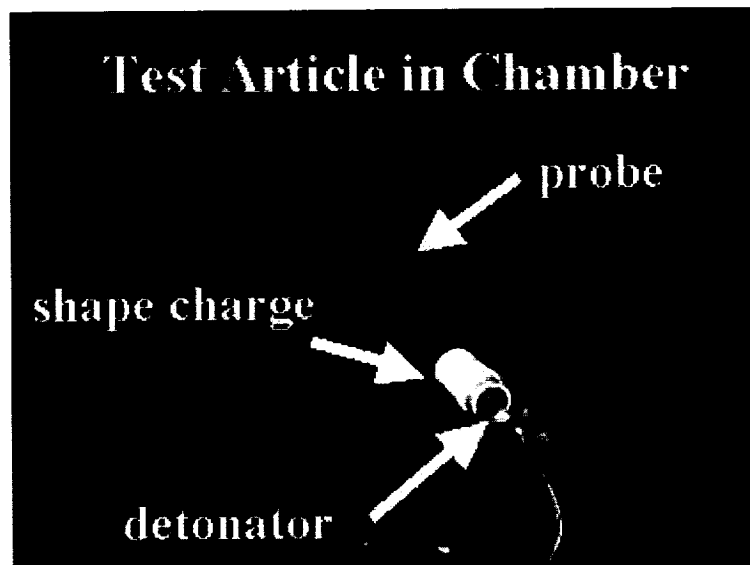
Figure 16. Photograph of assembled explosive unit in blast
chamber with attached detonator.

Representative time-of-flight waveforms from a typical test are shown in figure 17. The letter A denotes the first trip wire and letter B denotes the second trip wire. In this particular test without seed, the time of flight was 11 μsec, yielding a jet velocity of 9.1 km/sec, which is very near the anticipated value of 10 km/sec. The measured velocity invariably ranged between 9 and 10 km/sec with no dependence on seeding. The average time of flight from all usable test results was 11.2 μsec, yielding an average velocity of 9 km/sec.

To avoid any possible electrostatic effects on the probe measurements, the push-pull search coil configuration for all tests was utilized. Representative waveforms from a typical test are shown in figure 18. In this test, there was no seed in the charge, and the entire response occurred within 30 μsec. The peak signal amplitude is ≈22 V, and the push-pull signals are symmetric, as expected. The signal oscillations appear to be indicative of tears in the plasma jet due to a strong axial gradient in velocity. This result could be anticipated from the work of previous researchers in the field.

Waveforms obtained using seeded shaped charges were similar except the peak signal amplitudes ranged from 90 to 100 V. Representative push-pull pickup coil waveforms for a typical seeded explosive plasma jet are shown in figure 19. The increased peak voltage indicated a substantial increase in electrical conductivity, as expected.

In all cases, the entrance perturbation closely resembled a Gaussian response, indicating an abrupt and very strong increase in ionization behind the shock front. Attempts to perform Gaussian fits on the entrance perturbations for cases with and without seed are shown in figure 20. It is clear that the rising edge is more nearly Gaussian while the falling edge is extremely abrupt. However, the Gaussian does tend to fit slightly beyond the peak amplitude in all cases.
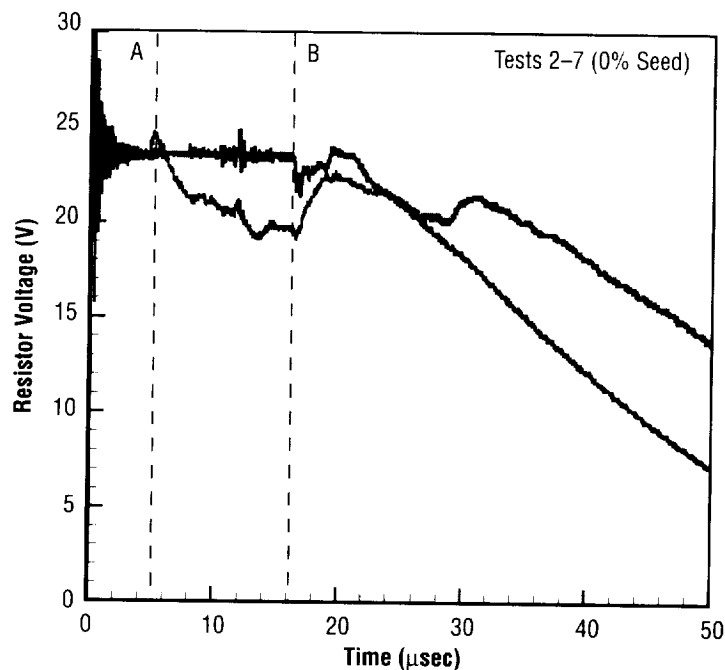

Figure 17. Representative time-of-flight waveform for typical explosive plasma jet.
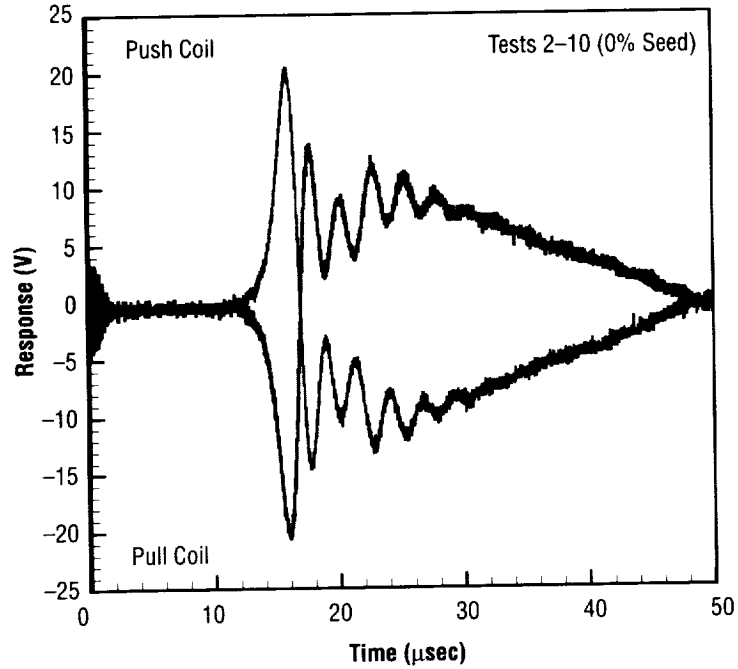
Figure 18. Representative push-pull pickup coil waveforms for typical unseeded explosive plasma jet.
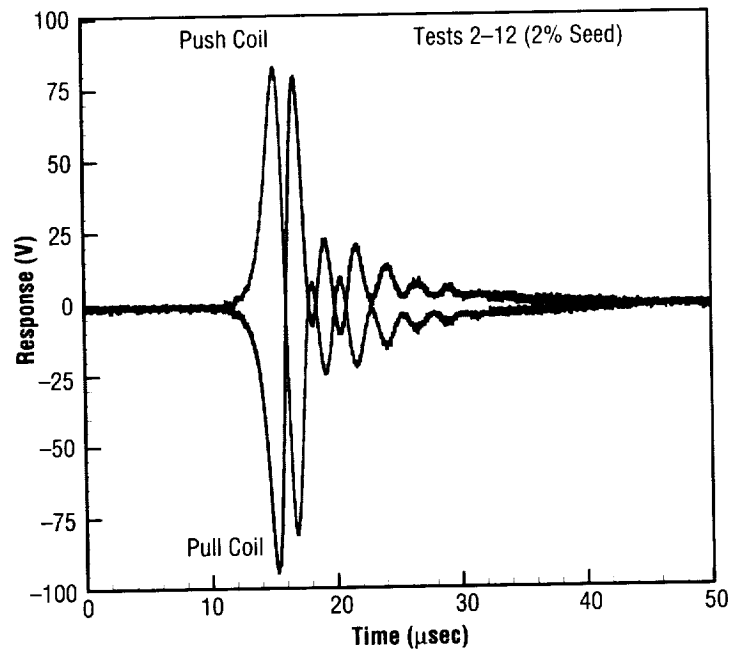
Figure 19. Representative push-pull pickup coil waveforms for typical seeded explosive plasma jet.

20
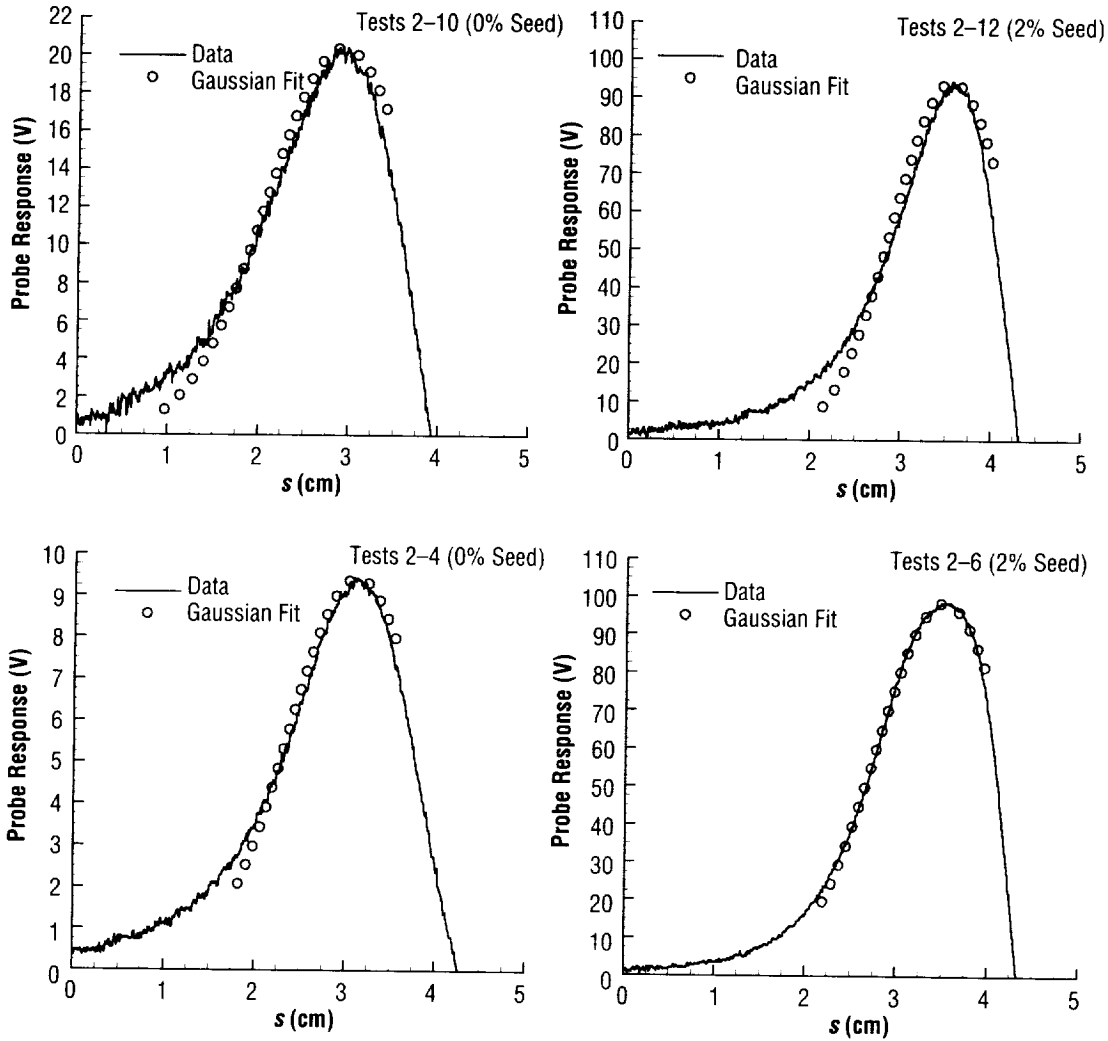
Figure 20. Gaussian fit to entrance perturbation signal for unseeded and seeded charges.

The results of four tests are summarized in tables 1 and 2 based on peak ratio and peak integral methods. Two are without seed and two are with seed. The measured jet velocities are also shown. Assuming that the entrance perturbations can be reasonably approximated by a Gaussian, peak electrical conductivity values in the plasma jet are inferred, using eq. (13), where it is implicitly assumed that ψ_1 is approximately unity. The results for the integral ratio method are based on eq. (14) with ψ_2 taken as unity. In general, the integral ratio method is a better approximation since ψ_2 exhibits less deviation from unity in all cases.

The peak electrical conductivity was found to be in the range of 4 kS/m for unseeded charges and in the range of 20 kS/m for seeded charges. Using the measured jet velocity, it was estimated that the product $\mu\sigma^* u$ may be as high as 46 m^{-1} for unseeded charges and 228 m^{-1} for seeded charges. This implies that significantly high values for the R_m in moderate-scale devices can be achieved; that is, devices which are measured in fractions of a meter. This implies that seeded shaped charges may be adequate for the proposed Mark I demonstration device.

Table 1. Summary of plasma jet measurements based
on the peak ratio method.

Parameter	Dimension	Peak Ratio Method ($\psi_1=1$)			
		2–4	2–10	2–6	2–12
Seeding	%	0	0	2	2
u	km/sec	9.1	10	9.5	9.1
σ^*/σ_c	10^{-5}	7.8	14	76	78
$\sigma^* u/\sigma_c u_c$	10^{-2}	3.3	6.5	34	33
σ^*	kS/m	2.6	4.6	25	26
$\mu\sigma^* u$	m^{-1}	29	58	300	295

Table 2. Summary of plasma jet measurements based
on the integral ratio method.

Parameter	Dimension	Integral Ratio Method ($\psi_2=1$)			
		2–4	2–10	2–6	2–12
Seeding	%	0	0	2	2
u	km/sec	9.1	10	9.5	9.1
σ^*/σ_c	10^{-5}	5.9	11	58	56
$\sigma^* u/\sigma_c u_c$	10^{-2}	2.5	5.1	26	24
σ^*	kS/m	1.9	3.6	19	18
$\mu\sigma^* u$	m^{-1}	22	46	228	210

22

6. CONCLUSIONS

An electrodeless inductive probe for measuring plasma jet electrical conductivity was designed, fabricated, calibrated, and tested. The 1-in.-diameter probe uses an excitation solenoid coil to produce an axisymmetric field within the bore, and a search coil is located nearby to detect field perturbations when the plasma jet enters the active probing region. The response function for the probe was obtained through a calibration procedure in which a metal slug of known conductivity was propelled through the probe with a known velocity. The signal obtained for an actual plasma jet experiment could then be used to determine conductivity through the inversion of a Fredholm integral equation of the first kind. A constrained linear inversion algorithm was developed for this purpose, but the results were only marginally successful. A more practical approach is to assume a conductivity distribution for which approximate analytical solutions are known.

Exploratory laboratory experiments were conducted using seeded and unseeded shaped charge explosives. The jet velocity was inferred from time-of-flight measurements and electrical conductivity determined from measurements using the inductive probe. The average jet velocity was ≈ 9 km/sec and the measured conductivities were in the range of 4 kS/m for unseeded charges and in the range of 26 kS/m for seeded charges. These values imply that seeded shaped charge explosive plasma jets can achieve magnetic Reynolds numbers significantly higher than unity in a moderate-scale device. This indicates that the proposed Mark I device built on a scale of fractions of a meter has a good chance of being successfully developed.

It is concluded that an inductive probing technique represents a very useful and reliable tool for investigating plasma jet ionization characteristics. Based on the results obtained in our exploratory experiments, it is further concluded that high-explosive plasma sources are capable of producing very high magnetic Reynolds number jets that can be of significant use in the development of magnetic flux compression reactors for pulsed nuclear/chemical propulsion and power. Additional experimental studies along these lines are recommended.

REFERENCES

1. Litchford, R.J.; Robertson, G.A.; Hawk, C.W.; Turner, M.W.; and Koelfgen, S.: "Magnetic Flux Compression Reactor Concepts for Spacecraft Propulsion and Power," *AIAA Paper 2000-2669*, 2000.

2. Burnham, M.W.; and Marshall, S.J.: "Some Experiments Related to Explosive Driven MHD Converters," *First Conference on Megagauss Magnetic Field Generation by Explosives and Related Experiments*, Frascati, Italy, H. Knoepfel and F. Herlach (eds.), Euratom publication *EUR 2750.e*, pp. 367–386, 1966.

3. Burnham, M.W.: "Explosive Parameters for Magnetohydrodynamic Energy Conversion," *Aeronautical Systems Division, Air Force Systems Command, Eglin Air Force Base, Final Report ASD–TDR–63–37*, Prepared by Falcon Research and Development Co. under contract No. AF 08(635)–2918, Sept. 1963.

4. Burnham, M.W.; and Marshall, S.J.: "Pulsed Electrical Power from Conventional Explosives," *Proc. of Int. Symposium on MHD Electrical Power Generation*, Paris, France, pp. 753–764, July 1964.

5. Jones, M.S.; and McKinnon, C.N.: "Explosive Driven Linear MHD Generators," *First Conference on Megagauss Magnetic Field Generation by Explosives and Related Experiments*, Frascati, Italy, H. Knoepfel and F. Herlach (eds.), Euratom publication *EUR 2750.e*, pp. 349–366, 1966.

6. Baum, D.W.; and Shimmin, W.L.: "Explosive Plasma Source Experiment," *Second Int. Conf. on Megagauss Magnetic Field Generation and Related Topics*, Washington, DC, P.J. Turchi (ed.), Megagauss Physics and Technology, Plenum Press, New York, pp. 77–88, 1980.

7. Voitenko, A.E.: "Generation of High-Speed Gas Jets," *Soviet Phys.—Doklady*, Vol. 9, No. 10, pp. 860–862, 1965.

8. Koski, W.S.; Lucy, F.A.; Shreffler, R.G.; and Willig, F.J.: "Fast Jets and Collapsing Cylinders," *J. App. Phys.*, Vol. 23, No. 12, pp. 1300–1305, 1952.

9. Wild, J.M.: "The Production of High-Velocity, High-Density Plasmas With Explosives," *General Atomics Report GA–2401*, July 1961.

10. Dunne, B.B.; Blackstead, A.W.; McKinney, W.B.; and Ritter, P.B.: "Mass of High Velocity Gases From Toroidal Implosion Charges," *General Atomics Report GAMD–3629*, Oct. 1962.

11. Lin, S.-C.; Resler, E.L.; and Kantrowitz, A.: "Electrical Conductivity of Highly Ionized Argon Produced by Shock Waves," *J. App. Phys.*, Vol. 26, No. 1, pp. 95–109, 1987.

12. Twomey, S.: *Introduction to the Mathematics of Inversion in Remote Sensing and Indirect Measurements*, American Elsevier, New York, 1977.

REPORT DOCUMENTATION PAGE	Form Approved OMB No. 0704-0188

Public reporting burden for this collection of information is estimated to average 1 hour per response, including the time for reviewing instructions, searching existing data sources, gathering and maintaining the data needed, and completing and reviewing the collection of information. Send comments regarding this burden estimate or any other aspect of this collection of information, including suggestions for reducing this burden, to Washington Headquarters Services, Directorate for Information Operation and Reports, 1215 Jefferson Davis Highway, Suite 1204, Arlington, VA 22202-4302, and to the Office of Management and Budget, Paperwork Reduction Project (0704-0188), Washington, DC 20503

1. AGENCY USE ONLY (Leave Blank)	2. REPORT DATE January 2001	3. REPORT TYPE AND DATES COVERED Technical Publication

4. TITLE AND SUBTITLE
Inductive Measurement of Plasma Jet Electrical Conductivity
(MSFC Center Director's Discretionary Fund Final Report;
Part II, Project No. 99–24)

5. FUNDING NUMBERS

6. AUTHORS
M.W. Turner,* C.W. Hawk,* and R.J. Litchford

7. PERFORMING ORGANIZATION NAMES(S) AND ADDRESS(ES)
George C. Marshall Space Flight Center
Marshall Space Flight Center, AL 35812

8. PERFORMING ORGANIZATION REPORT NUMBER
M–996

9. SPONSORING/MONITORING AGENCY NAME(S) AND ADDRESS(ES)
National Aeronautics and Space Administration
Washington, DC 20546–0001

10. SPONSORING/MONITORING AGENCY REPORT NUMBER
NASA/TP—2001–210794

11. SUPPLEMENTARY NOTES
Prepared by the Advanced Space Transportation Program, Space Transportation Directorate
*Propulsion Research Center, University of Alabama in Huntsville, Huntsville, AL

12a. DISTRIBUTION/AVAILABILITY STATEMENT
Unclassified-Unlimited
Subject Category 75
Standard Distribution

12b. DISTRIBUTION CODE

13. ABSTRACT (Maximum 200 words)

Measurement of plasma jet electrical conductivity has utility in the development of explosively driven magnetohydrodynamic (MHD) energy converters as well as magnetic flux compression reaction chambers for nuclear/chemical pulse propulsion and power. Within these types of reactors, the physical parameter of critical importance to underlying MHD processes is the magnetic Reynolds number, the value of which depends upon the product of plasma electrical conductivity and velocity. Therefore, a thorough understanding of MHD phenomena at high magnetic Reynolds number is essential, and methods are needed for the accurate and reliable measurement of electrical conductivity in high-speed plasma jets. It is well known that direct measurements using electrodes suffer from large surface resistances, and an electrodeless technique is desired. To address this need, an inductive probing scheme, originally developed for shock tube studies, has been adapted. In this method, the perturbation of an applied magnetic field by a plasma jet induces a voltage in a search coil, which, in turn, can be used to infer electrical conductivity through the inversion of a Fredholm integral equation of the first kind. A 1-in.-diameter probe was designed and constructed, and calibration was accomplished by firing an aluminum slug through the probe using a light-gas gun. Exploratory laboratory experiments were carried out using plasma jets expelled from 15-g shaped charges. Measured conductivities were in the range of 4 kS/m for unseeded octol charges and 26 kS/m for seeded octol charges containing 2-percent potassium carbonate by mass.

14. SUBJECT TERMS
plasmadynamics, plasma jet, electrical conductivity, experimental, high explosive, shaped charge, magnetic Reynolds number, electromagnetics

15. NUMBER OF PAGES
36

16. PRICE CODE
A03

17. SECURITY CLASSIFICATION OF REPORT Unclassified	18. SECURITY CLASSIFICATION OF THIS PAGE Unclassified	19. SECURITY CLASSIFICATION OF ABSTRACT Unclassified	20. LIMITATION OF ABSTRACT Unlimited

Standard Form 298 (Rev. 2-89)
Prescribed by ANSI Std 239-18
298-102